Available online at www.sciencedirect.com
SCIENCE DIRECT®
Thermochimica Acta 428 (2005) 31–39
thermochimica acta
www.elsevier.com/locate/tca

Enthalpy relaxation in the cooling/heating cycles of polypropylene/organosilica nanocomposites II. Melting behavior

V.P. Privalko*, R.V. Dinzhos, E.G. Privalko

Institute of Macromolecular Chemistry, National Academy of Sciences of Ukraine, 02160 Kyiv, Ukraine

Received 9 July 2004; accepted 24 September 2004

Abstract

Non-isothermally crystallized samples of the neat isotactic polypropylene homopolymer (PP-0) and of a series of nanocomposites (PNC) containing up to 4.68 vol.% of organosilica were characterized by wide-angle and small-angle X-ray diffraction and by the standard DSC, while their melting behavior was studied in the temperature-modulated DSC mode at three underlying heating rates and five modulation frequencies.

It was established that the lamellar morphology of PP remained essentially unchanged, whatever the previous cooling rate and/or the organoclay content. The patterns of melting endotherms in both the neat PP sample and the PNC could be semi-quantitatively characterized by a simple Debye model with a single, temperature- and underlying heating rate-dependent characteristic time. The mechanisms of structural rearrangements in the melting intervals of the neat PP sample and the PNC were basically similar; however, the spatial scale of such rearrangements in the latter samples was significantly reduced due to severe steric constraints on the PP chain mobility in the melt state from the infinite cluster of nanoparticles.

Keywords: Polypropylene nanocomposites; Enthalpy relaxation; Melting pattern; Debye model

1. Introduction

Theoretically, under isobaric conditions the ideal melting point T_m^0 of a crystallizable polymer partitions the two-dimensional phase space into temperature domains of stability of liquid (i.e., melt) and solid (crystal) states. The equilibrium melt above T_m^0 is macroscopically homogeneous in the sense that no inner interfaces are allowed to exist. In principle, the same argument should also apply in the temperature interval below T_m^0 to the ideal polymer crystal made up of completely extended chains (ECC). In practice, however, crystallization of flexible-chain polymers invariably proceeds via the formation of thermodynamically less stable (i.e., those melting at $T_m < T_m^0$) but kinetically more favorable folded-chain crystals (FCC) [1–3]. For this reason, the apparently solid polymers below T_m^0 are "semi-crystalline" in the sense that a substantial portion of material $(1 - X)$ (where X is the degree of crystallinity) remains in a disordered, non-crystalline state in the interstitial space between FCCs (lamellae).

Kinetic theory [3] predicts that the lamellar morphology of a semi-crystalline polymer is controlled by competition between the rate of deposition of secondary (surface) FCC nuclei on the crystal growth face and the rate of lateral spreading of such nuclei along that face. Depending on the degree of melt undercooling $\Delta T = T_m^0 - T$, crystallization may result in the formation of either a few large FCC (regime I at very low ΔT) or numerous small FCC

* Corresponding author. Tel.: +380 44 559 40 95; fax: +380 44 552 40 64.
E-mail address: privalko@iptelecom.net.ua (V.P. Privalko).

0040-6031/$ – see front matter © 2004 Elsevier B.V. All rights reserved.
doi:10.1016/j.tca.2004.09.019

(regime III at very high ΔT); the intermediate case of moderate ΔT corresponds to crystallization by regime II.

In principle, qualitative information on the initial morphology of a semi-crystalline polymer can be derived from the shape of a melting endotherm in the DSC heating run [4], provided the heating rate exceeds the rate of eventual structural rearrangements (i.e., under conditions of "zero entropy production" [5]). Otherwise, the expected DSC melting pattern can be distorted by contributions from other endo- or exothermal effects, such as local melting and recrystallization, superheating, etc. [6,7]. Nevertheless, such effects can be adequately accounted for with the temperature-modulated DSC (TM-DSC) either by separating the reversing and non-reversing components of the apparent specific heat capacity in the melting interval [8–10], or by analyzing its frequency and heating rate dependencies [11–13].

Our previous studies in the standard DSC mode [14] have revealed significant differences in both the nucleation parameters and the overall patterns of non-isothermal crystallization for the neat isotactic polypropylene and its organosilica nanocomposites. It is therefore the purpose of the present paper to study the melting behavior of these systems in the TM-DSC mode.

2. Experimental

The neat isotactic polypropylene (PP) homopolymer and the nanocomposites containing up to 4.68 vol.% of organosilica (samples PP-0, . . ., PP-4.68, respectively) were the same as those used in our previous studies [14–16].

The solid samples prepared under identical conditions of non-isothermal crystallization from the melt were characterized at room temperature by the wide-angle and small-angle X-ray scattering (WAXS and SAXS, respectively), as described in detail elsewhere [15,16].

Enthalpy relaxation during the heating runs was monitored in the temperature-modulated (TM) mode with the TM-DSC instrument (Perkin Elmer DSC-2, upgraded and supplied with signal processing software by the IFA GmbH, Ulm). Each sample was initially "overheated" by ∼50 K above the apparent melting temperature of PP ($T_m \approx 440$ K), stored for 3 min, cooled in the DSC mode at one of the two constant cooling rates q^- (20 or 0.5 K/min) to ∼360 K, stored isothermally for ca. 2 min and immediately heated up again in the TM mode at one of the three underlying heating rates $q^+ = 0.5$, 1 and 2 K/min (modulation amplitude: 0.1 K; modulation frequencies f: 10, 17, 33, 50 and 100 mHz). The calibration for determination of the total specific heat capacity (c_p) and of its reversing part (i.e., the complex specific heat capacity c_p^*) was carried out according to the recommended procedures [17,18] using a sapphire and a fused quartz as standards.

3. Results and discussion

3.1. Structural characterization of the initial samples

The overall patterns and the angular positions of crystalline reflections on the WAXS diagrams of both the neat PP-0 and all PNC (see the representative plots in Fig. 1a for samples prepared at $q^- = 16$ K/min) were identical to those for a typical isotactic PP [19]. The WAXS degrees of crystallinity XWAXS as well as the effective dimensions of crystalline PP lamellae $\langle l_{WAXS} \rangle$ (estimated from broadening

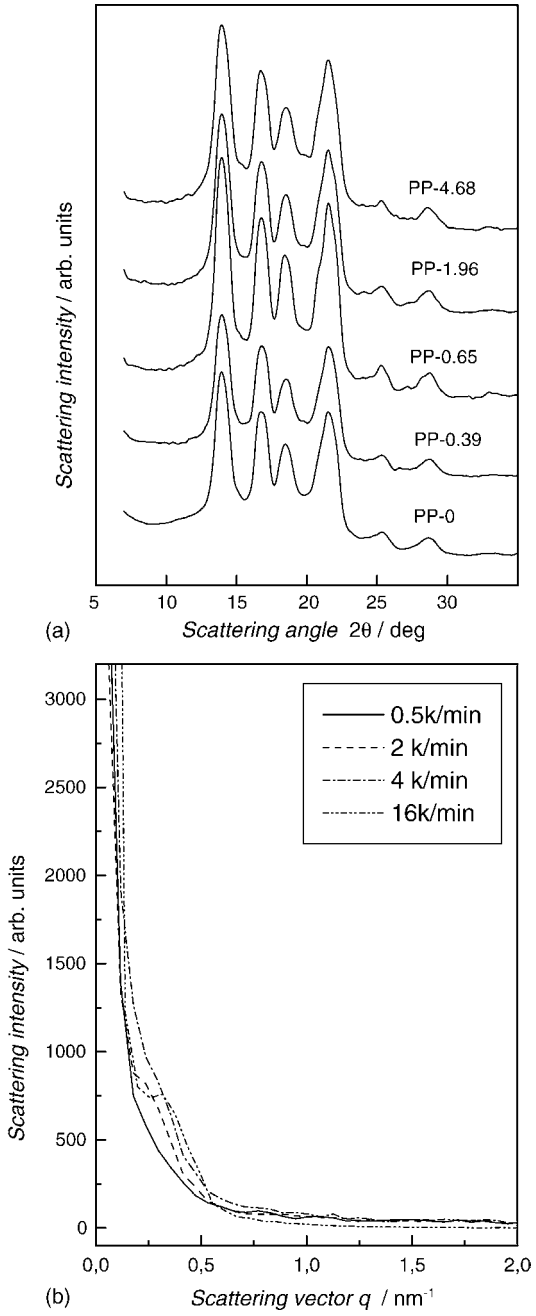

Fig. 1. WAXS patterns for samples of series 1 (a) and SAXS patterns for PP-0 prepared at the indicated cooling rates (b).

Table 1
Structural parameters derived from the WAXS data

Samples	q^- (K/min)							
	0.5		2		4		16	
	X_{WAXS}	$\langle l_{WAXS}\rangle$ (nm)	X_{WAXS}	$\langle l_{WAXS}\rangle$ (nm)	X_{WAXS}	$\langle l_{WAXS}\rangle$ (nm)	X_{WAXS}	$\langle l_{WAXS}\rangle$ (nm)
PP-0	0.68	7.4	0.67	7.7	0.67	7.3	0.66	7.5
PP-0.39	0.69	7.5	0.68	7.5	0.67	7.4	0.66	7.6
PP-0.65	0.68	7.4	0.68	7.6	0.67	7.5	0.66	7.5
PP-1.96	0.67	7.3	0.68	7.4	0.67	7.5	0.66	7.3
PP-4.68	0.67	7.1	0.67	7.0	0.67	7.2	0.65	6.8

of the crystal d_{110} reflection at $2\theta \approx 14^\circ$ by Sherrer's formula) tended to decrease slightly, the higher the q^- for both PP-0 and PNC; each of these parameters, however, turned out essentially composition-invariant (Table 1). A similar conclusion could be made for the DSC degrees of crystallinity ($X_{DSC} = \Delta H_m/\Delta H_m^0 = 0.68 \pm 0.03$, where ΔH_m and ΔH_m^0 (=165.2 J/g) [4] are the melting enthalpies of a semicrystalline sample and of a completely crystalline isotactic PP, respectively). It can be inferred from these data that the lamellar morphology of PP remained unchanged, whatever the previous cooling rate and/or the organoclay content.

As typical for unoriented semi-crystalline polymers with stacks of FCC lamellae separated by non-crystalline material in the interstitial space [19], the well-resolved SAXS reflection near the scattering vector $q \approx 0.325\,nm^{-1}$ for PP-0 at $q^- = 16$ K/min (Fig. 1b) tended to shift to lower values of q (i.e., the corresponding Bragg's periodicities increased), the lower the previous cooling rate q^- (Fig. 1b). This reflec-

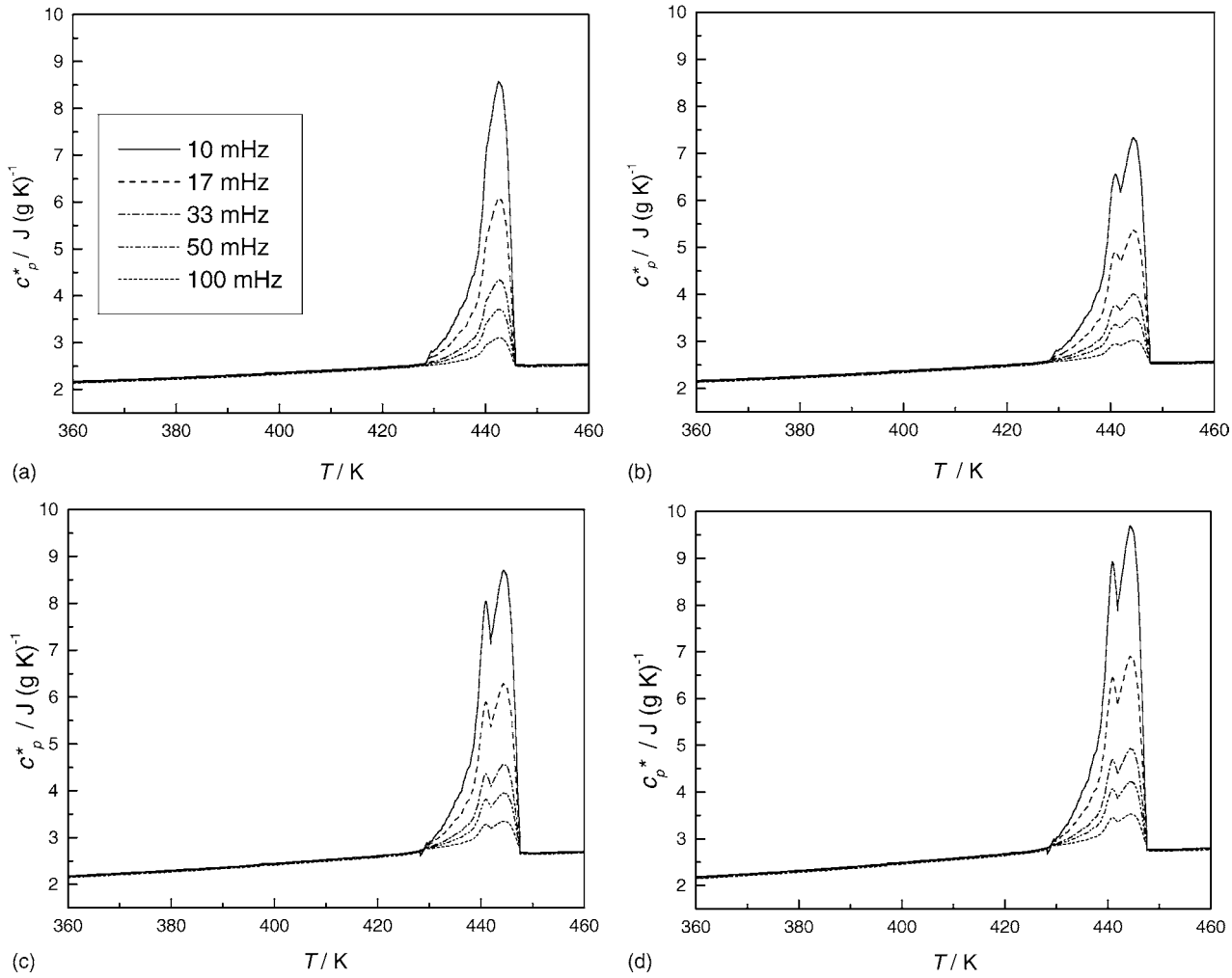

Fig. 2. Complex specific heat capacities of PP-0 prepared at the cooling rates of 0.5°/min (a), 2°/min (b), 10°/min (c) and 20°/min (d) (underlying heating rate: 0.5°/min).

tion, however, could not be resolved on the SAXS curves of PNC due to the sharp increase of SAXS intensity in the same range of scattering vectors. These results suggest a significant increase of structural heterogeneity due to the appearance of new, strongly scattering entities (presumably, polymer-nanoparticle interfaces and microvoids) with broad distribution of their sizes [14,15].

3.2. Kinetics of melting

The common features of the heating runs for both PP-0 and the PNC were the initial smooth increases of both c_p and c_p^* in the solid state followed by sharp melting endotherms and final apparent leveling-offs in the melt state (see the representative plots for PP-0 in Fig. 2). For samples prepared by cooling at $q^- = 0.5\,\mathrm{K/min} \leq q^+$ (hereafter referred to as series 1) the melting endotherms were virtually unimodal, passing through a single maximum at the apparent melting point T_m, whereas for samples prepared by cooling at $q^- = 20\,\mathrm{K/min} \gg q^+$ (series 2) one could observe not only the main melting peak at T_m but also the appearance and gradual gain in the intensity of a subsidiary maximum at $T'_\mathrm{m} < T_\mathrm{m}$. It followed from this latter result that structural rearrangements in the course of heating through the melting interval were more pronounced in the samples of series 2.

As can be seen from Fig. 3, both the reversing, excess specific heat capacities c_p^*, as well as the corresponding peak areas within the melting intervals of the PNC were not only smaller than those for the neat polymer sample PP-0, but systematically decreased, the higher the organoclay content. This effect can be attributed to severe steric constraints on the PP chain mobility in the melt state of the PNC from the infinite clusters of nanoparticles [15,16].

As expected, the reversing specific heat capacities c_p^* outside the temperature interval of melting were modulation frequency-invariant, while within that interval the values of

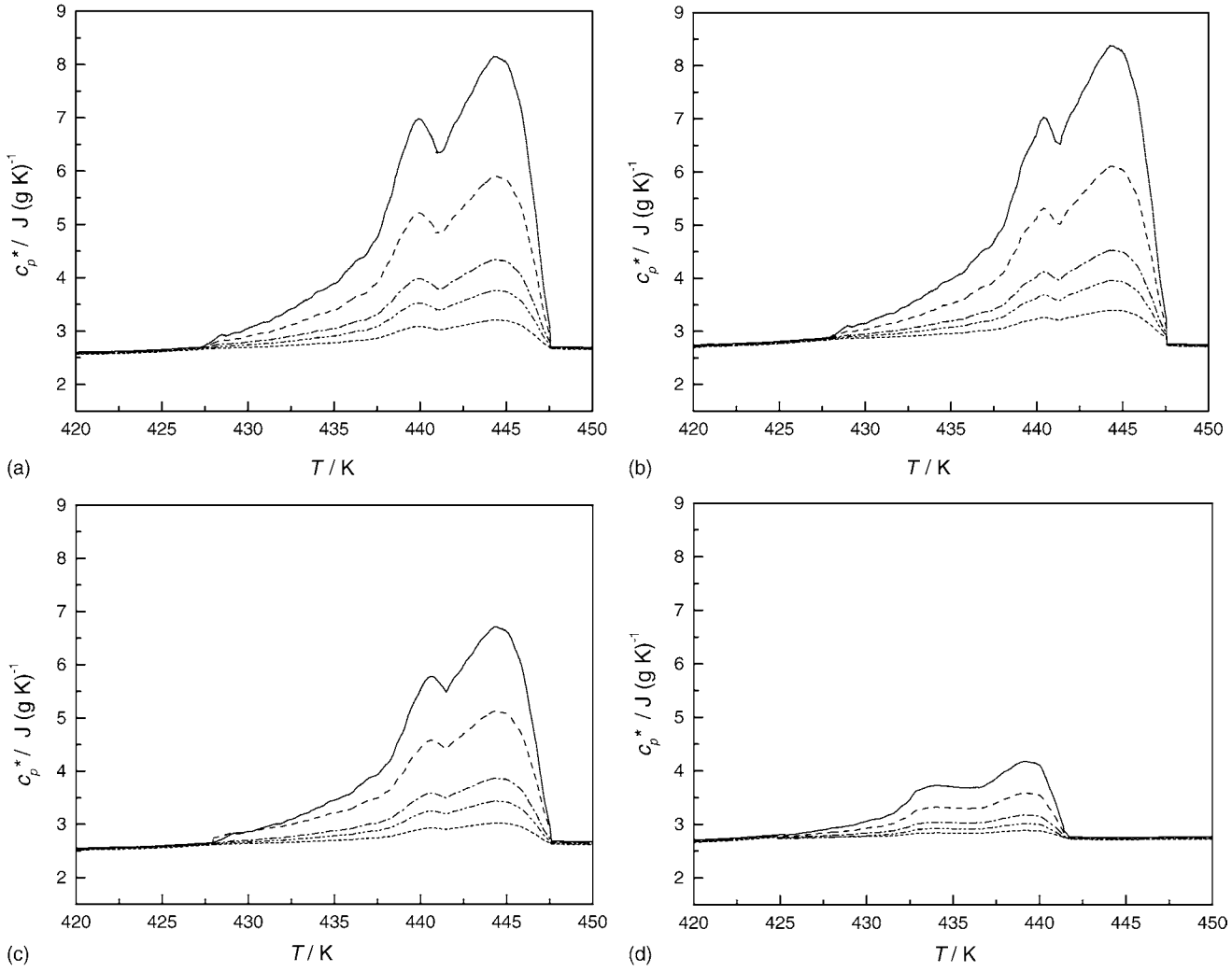

Fig. 3. Complex specific heat capacities in the melting intervals of PP-0.39 (a), PP-0.65 (b), PP-1.96 (c) and PP-4.68 (d) prepared at the cooling rate of 20°/min (underlying heating rate: 0.5°/min).

c_p^*, as well as the corresponding peak areas tended to decrease, the higher the modulation frequency (Fig. 3). Similar behavior was also observed for the real (c_p') and the imaginary (c_p'') components of the complex specific heat capacity, $c_p^* = c_p' - \mathrm{i}c_p''$ (Fig. 4). These results implied that the characteristic times (τ) for structural rearrangements involved were comparable to the modulation periods (i.e., reciprocal frequencies).

In terms of the standard definition [11],

$$c_p'(\omega) = c_{\mathrm{st}} + c_{\mathrm{dyn}}'(\omega), \tag{1a}$$

$$c_p''(\omega) = c_{\mathrm{dyn}}''(\omega), \tag{1b}$$

it is the dynamic parts of real and imaginary components of c_p^* [$c_{\mathrm{dyn}}'(\omega)$ and $c_{\mathrm{dyn}}''(\omega)$, respectively] which account for its response to the circular modulation frequency ω in the

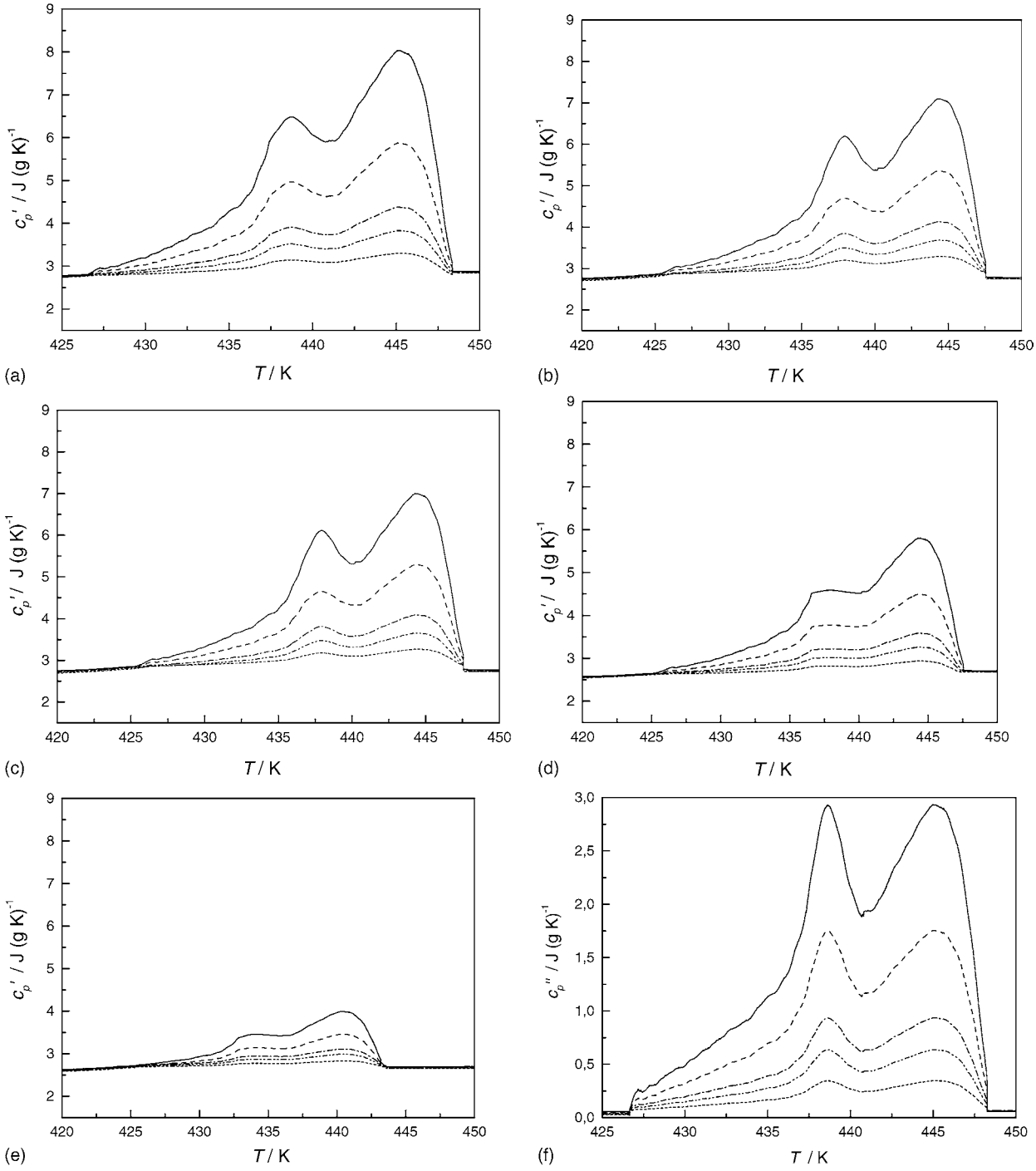

Fig. 4. Real (a–e) and imaginary (f–j) components of the complex specific heat capacities of PP-0 (a and f), PP-0.39 (b and g), PP-0.65 (c and h), PP-1.96 (d and i) and PP-4.68 (e and j) prepared at the cooling rate of 20°/min (underlying heating rate: 2°/min).

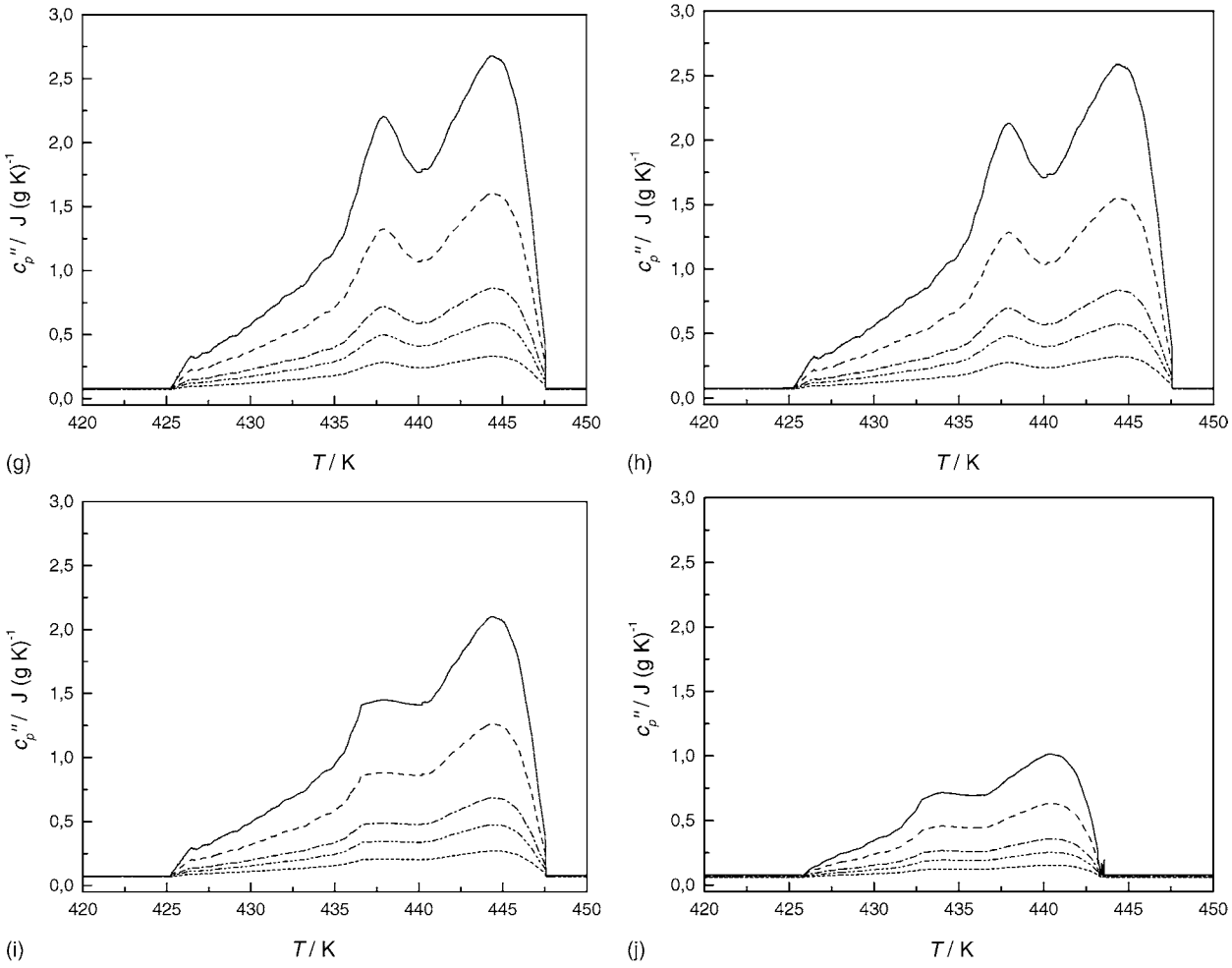

Fig. 4. (*Continued*).

melting interval. Assuming that this response is Debye-like, one can write [11–13]

$$c^*_{\mathrm{dyn}}(\omega) = c'_{\mathrm{dyn}}(\omega) - \mathrm{i}c''_{\mathrm{dyn}}(\omega) = \frac{\mathrm{HF}}{1+\mathrm{i}\omega\tau} = \frac{\mathrm{HF}(1-\mathrm{i}\omega\tau)}{(1+\mathrm{i}\omega\tau)(1-\mathrm{i}\omega\tau)} = \frac{\zeta_0\tau}{1+\omega^2\tau^2} + \frac{\mathrm{i}\zeta_0\omega\tau^2}{1+\omega^2\tau^2}, \tag{2a}$$

$$c'_{\mathrm{dyn}}(\omega) = c'_p(\omega) - c_{\mathrm{st}} = \frac{\zeta_0\tau}{1+\omega^2\tau^2}, \tag{2b}$$

$$c''_{\mathrm{dyn}}(\omega) = \frac{\zeta_0\omega\tau^2}{1+\omega^2\tau^2}, \tag{2c}$$

where HF (=$\tau\zeta_0$) is the heat flow rate, τ the characteristic time, and ζ_0 the rate constant of the relevant structural rearrangements.

The experimental values of $c'_{\mathrm{dyn}}(\omega)$ and $c''_{\mathrm{dyn}}(\omega)$ at all three underlying heating rates were treated by Eq. (2a) to derive the best-fit values of ζ_0 and τ which were, finally, used to construct the corresponding Debye master plots [the values of $c'_{\mathrm{dyn}}(\omega)$ were evaluated by Eq. (2b) assuming that the static parts c_{st} corresponded to the baselines connecting the start- and the end-points of melting endotherms in Fig. 4]. As can be inferred from inspection of Fig. 5, the frequency-dependent patterns of melting endotherms in all studied samples can be semi-quantitatively characterized by a simple Debye model; however, the appreciable scatter of the data points suggests that the fitting parameters ζ_0 and τ are, in fact, the average values for several overlapping mechanisms of structural rearrangements involved.

Similar by magnitude characteristic times τ for both the neat PP sample and the PNC (Table 2) imply basically similar mechanisms of the relevant structural rearrangements, while several-fold smaller values of $c'_{\mathrm{dyn}}(\omega)$ and $c''_{\mathrm{dyn}}(\omega)$, as well as of the fitting parameters ζ_0 from Eq. (2a) for the PNC suggest considerably reduced spatial scale of such rearrangements. Regrettably, the limited range of the available underlying heating rates makes impossible the quantitative assessment of $\tau(q^+)$ relationships [11–13] for studied samples.

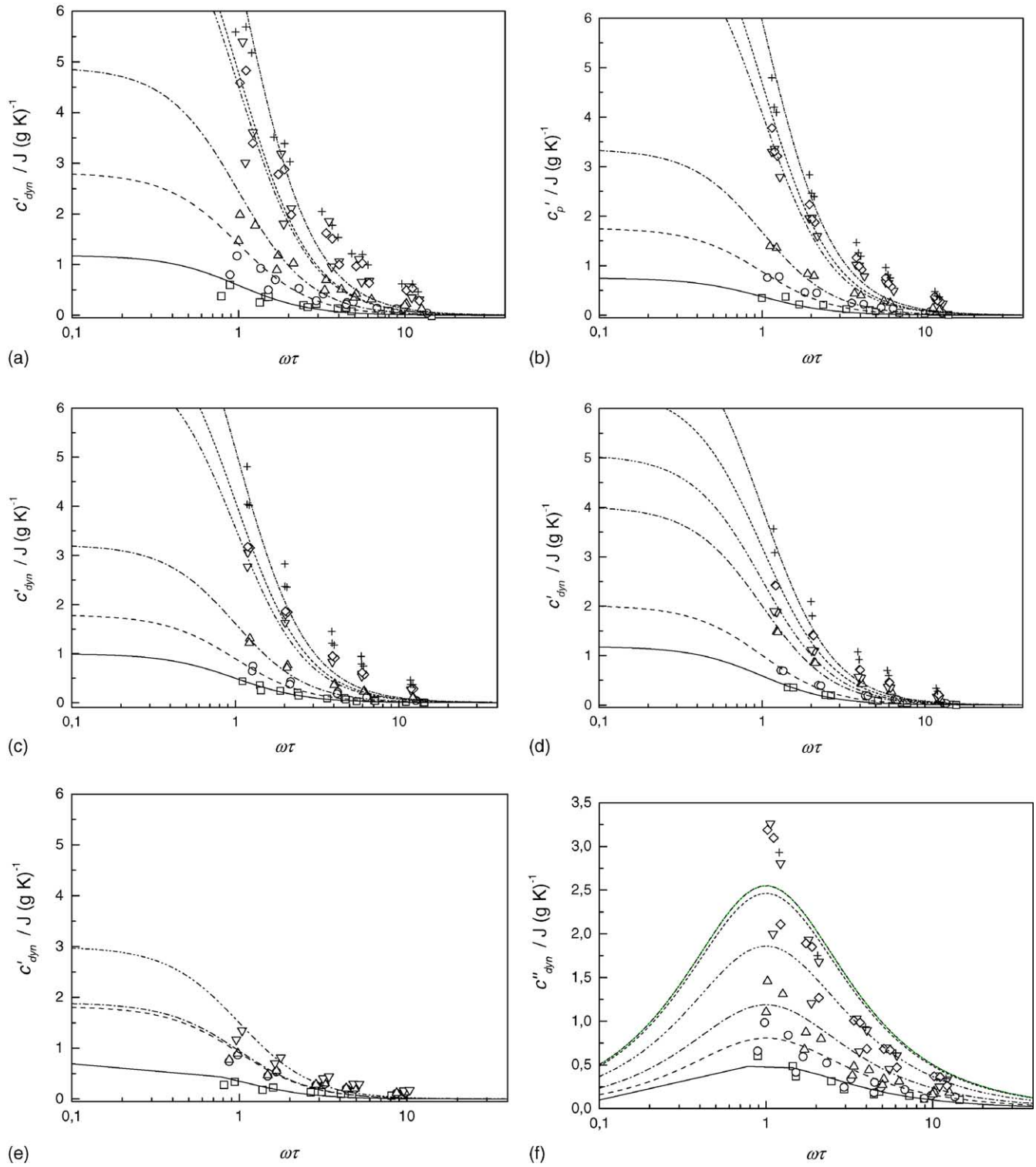

Fig. 5. Debye master plots for the real (a–e) and imaginary (f–j) components of the complex specific heat capacities at 430 K (squares), 433 K (circles), 436 K (up triangles), 439 K (down triangles), 442 K (diamonds) and 445 K (crosses) for PP-0 (a and f), PP-0.39 (b and g), PP-0.65 (c and h), PP-1.96 (d and i) and PP-4.68 (e and j) prepared at the cooling rate of 20°/min.

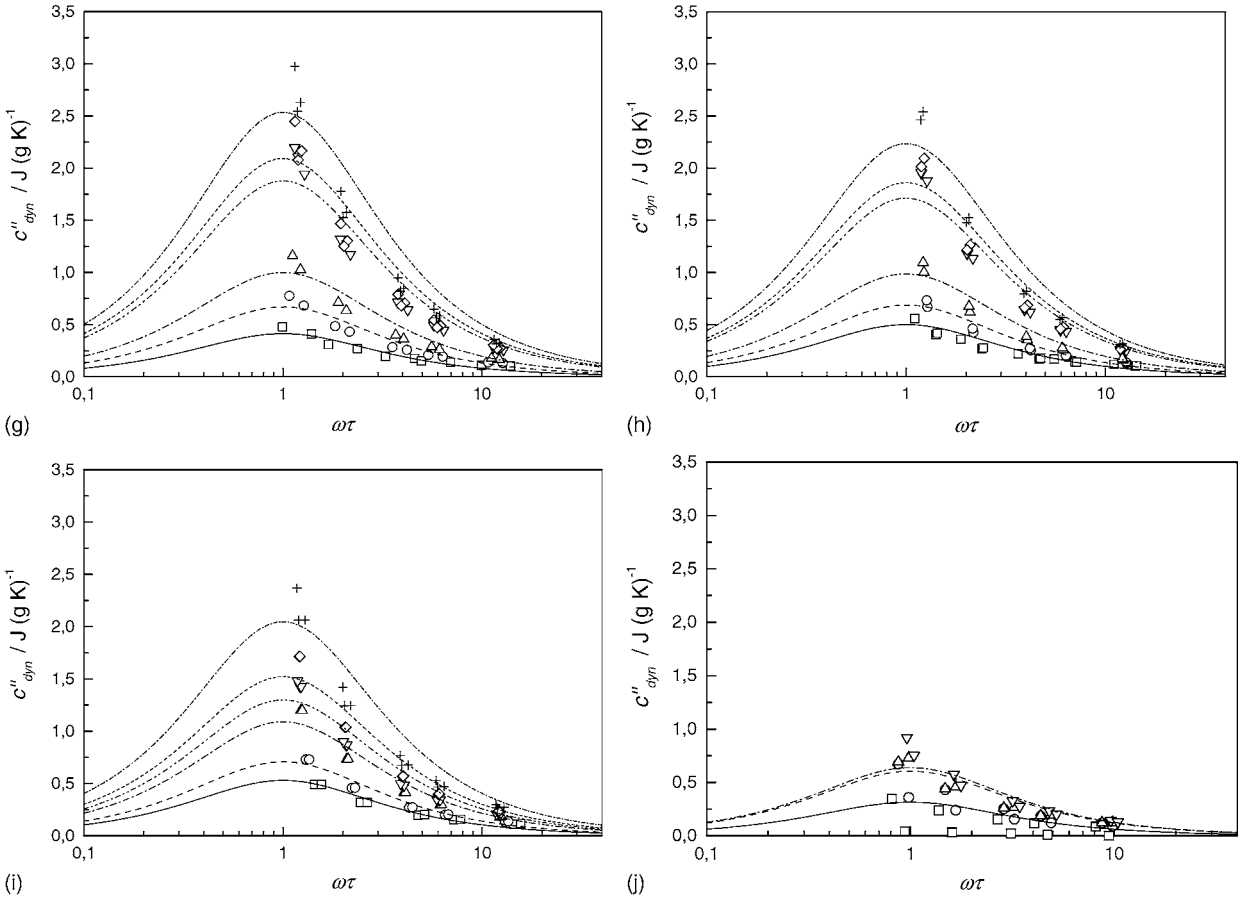

Fig. 5. (*Continued*).

Table 2
Characteristic times (s) of structural rearrangements in the melting intervals

T (K)	q^-/q^+					
	0.5/0.5	0.5/1.0	0.5/2.0	20/0.5	20/1.0	20/2.0
PP-0						
430	115	–	78	79	89	145
433	117	–	85	89	98	136
436	117	120	103	100	102	126
439	117	118	108	110	106	122
442	117	115	108	111	102	122
445	117	117	–	111	96	120
PP-0.39						
430	107	136	167	100	139	–
433	114	126	100	108	127	145
436	115	121	145	112	122	129
439	116	119	167	145	199	128
442	116	117	167	145	199	124
445	116	117	–	145	199	122
PP-0.65						
430	105	–	116	144	141	–
433	113	106	109	127	128	142
436	114	111	105	122	123	128
439	115	113	104	119	119	127
442	116	115	104	118	119	123
445	116	115	–	118	118	122

Table 2 (*Continued*)

T (K)	q^-/q^+					
	0.5/0.5	0.5/1.0	0.5/2.0	20/0.5	20/1.0	20/2.0
PP-1.96						
430	–	–	120	134	156	144
433	100	103	120	124	135	130
436	108	110	117	121	125	123
439	111	112	117	118	123	122
442	114	115	117	118	122	120
445	114	115	–	117	129	120
PP-4.68						
430	91	–	157	94	–	81
433	93	96	148	98	81	87
436	96	106	128	98	94	87
439	98	110	123	104	106	96
442	–	114	125	–	107	94
445	–	115	–	–	110	–

4. Conclusions

1. The lamellar morphology of PP remains essentially unchanged, whatever the previous cooling rate and/or the organoclay content.
2. The patterns of melting endotherms in both the neat PP sample and the PP-organosilica nanocomposites can

be semi-quantitatively characterized by a simple Debye model with a single, temperature- and underlying heating rate-dependent characteristic time.

3. The mechanisms of structural rearrangements in the melting intervals of the neat PP sample and the PNC are basically similar; however, the spatial scale of such rearrangements in the latter samples is significantly reduced due to severe steric constraints on the PP chain mobility in the melt state from the infinite cluster of nanoparticles.

Acknowledgements

Thanks are due to the International Bureau of the BMBF (Germany) for financial support of upgrading the DSC-2 instrument, and to Prof. C. Schick and his group (University of Rostock, Germany) for offering their expertise in operating the temperature-modulated DSC.

References

[1] P.H. Geil, Polymer Single Crystals, Interscience, New York, 1963.
[2] A. Keller, Polymer crystals, Rep. Prog. Phys. 31 (1968) 623–704.
[3] J.D. Hoffman, G.T. Davis, J.I. Lauritzen, The rate of crystallization of linear polymers with chain folding, in: N.B. Hannay (Ed.), Treatise on Solid State Chemistry, vol. 3, Plenum Press, New York, 1976, pp. 497–614.
[4] H.-G. Kilian, The non-homogeneous thermodynamically autonomous and equivalent microphases, Prog. Coll. Polym. Sci. 72 (1986) 60–82.
[5] B. Wunderlich, Crystal Melting: Macromolecular Physics, vol. 3, Academic Press, New York, 1980.
[6] V.A. Bershtein, V.M. Egorov, Differential Scanning Calorimetry in the Physical Chemistry of Polymers, Khimia, Leningrad, 1990 (in Russian).
[7] B. Wunderlich, Reversible crystallization and the rigid-amorphous phase in semicrystalline macromolecules, Prog. Polym. Sci. 28 (2003) 383–450.
[8] W.G. Kampert, B.B. Sauer, Temperature modulated DSC studies of melting and recrystallization in poly(ethylene-2,6-naphthalene dicarboxylate) (PEN) and blends with poly-(ethylene terephthalate), Polymer 42 (2001) 8703–8714.
[9] Z. Qiu, M. Komura, T. Ikehara, T. Nishi, DSC and TMDSC study of melting behavior of poly(butylenes succinate) and poly(ethylene succinate), Polymer 44 (2003) 7781–7785.
[10] C.-L. Wei, M. Chen, F.-E. Yu, Temperature modulated DSC and DSC studies on the origin of double melting peaks in poly(ether ether ketone), Polymer 44 (2003) 8185–8193.
[11] J.E.K. Schawe, E. Bergmann, Investigation of polymer melting by temperature modulated differential scanning calorimetry and its description using kinetic models, Thermochim. Acta 304–305 (1997) 179–186.
[12] A. Toda, C. Tomita, M. Hikosaka, Temperature modulated DSC of irreversible melting of nylon 6 crystals, J. Therm. Anal. 54 (1998) 623–635.
[13] A. Toda, C. Tomita, M. Hikosaka, Y. Saruyama, Kinetics of irreversible melting of polyethylene crystals revealed by temperature modulated DSC, Thermochim. Acta 324 (1998) 95–107.
[14] V.P. Privalko, R.V. Dinzhos, E.G. Privalko, Enthalpy relaxation in the cooling/heating cycles of polypropylene/organosilica nanocomposites. I. Non-isothermal crystallization, Thermochim. Acta, in press.
[15] V.P. Privalko, V.M. Karaman, E.G. Privalko, R. Walter, K. Friedrich, M.Q. Zhang, M.Z. Rong, Structure and thermoelasticity of irradiation grafted nano-inorganic particle filled polypropylene composites in the solid state, J. Macromol. Sci. Phys. 41B (2002) 485–503.
[16] V.M. Karaman, Thermo- and viscoelasticity of thermoplastic nanocomposites on the basis of polypropylene and polyamide 6, Ph.D. Thesis, Institute of Macromolecular Chemistry, National Academy of Sciences of Ukraine, Kyiv, 2003.
[17] B. Wunderlich, A. Boller, I. Okazaki, K. Ishikiriyama, Heat capacity determination by temperature-modulated DSC and its separation from transition effects, Thermochim. Acta 304–305 (1997) 125–136.
[18] M. Ribeiro, J.-P.E. Grolier, Temperature modulated DSC for the investigation of polymer materials. A brief account of recent studies, J. Therm. Anal. Calorim. 57 (1999) 253–263.
[19] B. Wunderlich, Crystal Structure, Morphology, Defects: Macromolecular Physics, vol. 1, Academic Press, New York, 1973 (Chapter IV).